Received: 15 April 2024 | Revised: 29 July 2024 | Accepted: 30 July 2024

DOI: 10.1002/pmic.202300591

Proteomics
Proteomics and Systems Biology

RESEARCH ARTICLE

Diabetic retinopathy from the vitreous proteome perspective: The *INS*^{C94Y} transgenic pig model study

Roxane L. Degroote[1] | **Adrian Schmalen**[1] | **Simone Renner**[2,3,4] | **Eckhard Wolf**[2,3,4,5] | **Stefanie M. Hauck**[6] | **Cornelia A. Deeg**[1]

[1]Chair of Physiology, Department of Veterinary Sciences, LMU Munich, Munich, Germany

[2]Chair for Molecular Animal Breeding and Biotechnology, Department of Veterinary Sciences, LMU Munich, Munich, Germany

[3]Center for Innovative Medical Models (CiMM), Department of Veterinary Sciences, LMU Munich, Munich, Germany

[4]German Center for Diabetes Research (DZD), Neuherberg, Germany

[5]Laboratory for Functional Genome Analysis (LAFUGA), Gene Center, LMU Munich, Munich, Germany

[6]Metabolomics and Proteomics Core, Helmholtz Center Munich, German Research Center for Environmental Health, Munich, Germany

Correspondence
Cornelia A. Deeg, Chair of Physiology, Department of Veterinary Sciences, LMU Munich, 82152 Martinsried, Munich, Germany.
Email: cornelia.deeg@lmu.de

Funding information
German Center for Diabetes Research (DZD), Grant/Award Number: 82DZD08D03SPP (to E.W.); Deutsche Forschungsgemeinschaft, Grant/Award Numbers: SPP 2127, DFG DE 719/7-1 (to C.A.D)

Abstract

INS^{C94Y} transgenic pigs represent a model for mutant insulin gene-induced diabetes of youth, with impaired insulin secretion and beta cell loss, leading to elevated fasting blood glucose levels. A key complication of diabetes mellitus is diabetic retinopathy (DR), characterized by hyperglycemia-induced abnormalities in the retina. Adjacent to the retina lies the vitreous, a gelatinous matrix vital for ocular function. It harbors proteins and signaling molecules, offering insights into vitreous biology and ocular health. Moreover, as a reservoir for secreted molecules, the vitreous illuminates molecular processes within intraocular structures, especially under pathological conditions. To uncover the proteomic profile of porcine vitreous and explore its relevance to DR, we employed discovery proteomics to compare vitreous samples from *INS*^{C94Y} transgenic pigs and wild-type controls. Our analysis identified 1404 proteins, with 266 showing differential abundance in *INS*^{C94Y} vitreous. Notably, the abundances of ITGB1, COX2, and GRIFIN were significantly elevated in *INS*^{C94Y} vitreous. Gene Set Enrichment Analysis unveiled heightened MYC and mTORC1 signaling in *INS*^{C94Y} vitreous, shedding light on its biological significance in diabetes-associated ocular pathophysiology. These findings deepen our understanding of vitreous involvement in DR and provide valuable insights into potential therapeutic targets. Raw data are accessible via ProteomeXchange (PXD038198).

KEYWORDS
diabetic retinopathy, *INS*^{C94Y} transgenic pig, vitreous proteome

1 | INTRODUCTION

The vitreous humor, a gel-like substance in the posterior segment of the eye, is more than an inert structure with purely anatomical significance. It was long viewed merely as structural support for the shape of the eyeball. However, it is now known to harbor a complex microenvironment that contributes to ocular homeostasis through various proteins [1]. Due to its immediate proximity to the lens and retina, proteins are

Abbreviations: COX2, cytochrome c oxidase subunit 2; DR, diabetic retinopathy; ER, endoplasmic reticulum; GRIFIN, Galectin-Related Inter-Fiber Protein; GSEA, Gene Set Enrichment Analysis; INS, insulin; ITGB1, integrin β1; MIDY, mutant *INS* gene-induced diabetes of youth; mTORC1, mechanistic target of rapamycin complex 1; MYC, myelocytomatosis oncogene; UPR, unfolded protein response; wt, wild-type.

also secreted into the vitreous from these structures [2]. This reservoir thus influences not only physiological ocular homeostasis but also can indicate pathological processes in these adjacent tissues.

Diabetic retinopathy (DR) and cataracts are severe complications manifesting in eyes of individuals with diabetes mellitus, which eventually lead to vision loss [3]. Especially in the retina, hyperglycemia-induced microvascular damage leads to pathological changes including retinal neovascularization, retinal hemorrhage, and macula edema [3].

Respective important ocular abnormalities observed in diabetes mellitus also develop in *INS*^{C94Y} transgenic pigs [4]. Due to this pathophysiological similarity as well as strong parallels in anatomy, physiology, metabolism and lifespan, the *INS*^{C94Y} pig serves as a valuable large animal model with significant translational potential for pathologies induced through persistent hyperglycemia in humans [5, 6].

In this study, we used a shotgun proteomics approach to comprehensively analyze the vitreous humor proteome of *INS*^{C94Y} pigs and wild-type (wt) littermates with a minimum age of 24 months. Through differential proteomics and subsequent Gene Set Enrichment Analysis (GSEA) we aimed at gaining insights into the impact of long-term chronic hyperglycemia on the vitreous proteome, in order to assess its role in the pathophysiology of diabetic cataract and DR. Since the vitreous is more readily accessible in diabetes patients than other ocular tissues, it has potential as a tool for diagnostic purposes or to target and pharmacologically influence factors contributing to the pathology of diabetic cataracts or the development of DR.

Significance Statement

Because the vitreous is more easily accessible than other ocular tissues, it is a promising substrate for diagnostics and therapeutic delivery strategies in patients with ophthalmic disorders, such as cataract and retinopathy. Due to strong similarities in anatomy, physiology and ocular pathology, the *INS*^{C94Y} pig holds significant translational potential for studying hyperglycemia-induced eye disorders in patients with mutant *INS* gene-induced diabetes of youth (MIDY). Providing insights into the proteomic profile of the vitreous in this transgenic pig model contributes to a better understanding of the mechanisms driving severe ocular complications associated with persistent hyperglycemia in diabetes mellitus, underlining its potential as a valuable tool for early detection and targeted treatment.

2 | MATERIALS AND METHODS

2.1 | Vitreous processing of *INS*^{C94Y} pigs and wild-type controls

Vitreous of six *INS*^{C94Y} pigs and six age-matched wt littermates were used in this study (age 24 months, female: five *INS*^{C94Y} pigs, five wt pigs; age 40 months, male: one *INS*^{C94Y} pig, one wt pig). *INS*^{C94Y} and wt pigs were generated at the Center for Innovative Medical Models (CiMM), LMU Munich, Germany. The generation of the *INS*^{C94Y} pig model as well as its main pathophysiological features have been comprehensively described [4–7]. Briefly, *INS*^{C94Y} pigs showed progressively decreasing mass of pancreatic β-cells, impaired insulin secretion resulting in chronic hyperglycemia and reduced growth compared to wt littermates [6]. Moreover, these pigs developed lens cataracts and severe retinopathy with retinal edema, vascular abnormalities, and several features characteristic of proliferative DR in humans [4, 6]. All animal experiments were performed according to the German Animal Welfare Act and were permitted by local authorities (Regierung von Oberbayern, permit ROB 55.2-1-54-2532-68-11). Pigs were kept under controlled conditions with daily blood glucose monitoring and received low-dose insulin treatment to maintain moderate hyperglycemia [8]. Immediately after euthanasia of pigs, eyes were enucleated and 1 mL vitreous was obtained from either one or both eyes using a hypodermic needle and a syringe, resulting in 11 samples per group, which were instantly frozen and stored at −20°C until further processing. At the time of sampling, the *INS*^{C94Y} pigs used in this study had chronic hyperglycemia [8]. Ocular findings in *INS*^{C94Y} pigs included signs of DR such as extraretinal hemorrhage, cotton-wool spots, and intraretinal vessel abnormalities [4]. Further, we observed mature cataracts and retinal abnormalities such as increased retinal thickness especially in the nerve fibre/ganglion cell layer (Figure S1), which were previously shown in the same animals [4]. The combination of these ocular anomalies are hallmarks of the *INS*^{C94Y} pig model phenotype [5, 6].

2.2 | Mass spectrometric analysis

From each of the 22 samples, 10 µg total protein was digested with LysC and trypsin by filter-aided sample preparation (FASP) as described [9]. Acidified eluted peptides were analyzed in the data-dependent mode on a Q Exactive HF mass spectrometer (Thermo Fisher Scientific, Dreieich, Germany) online coupled to a UItimate 3000 RSLC nano-HPLC (Dionex/Thermo Fisher Scientific, Dreieich, Germany). Samples were automatically injected and loaded onto the C18 trap cartridge and, after 5 min, eluted and separated on the C18 analytical column (nanoEase MZ HSS T3, 100 Å, 1,8 µm, 75 µm x 250 mm; Waters, Eschborn, Germany) by a 95-min nonlinear acetonitrile gradient at a flow rate of 250 nL/min. MS spectra were recorded at a resolution of 60,000 with an automatic gain control (AGC) target of $3e^6$ and a maximum injection time of 30 ms from 300 to 1500 *m/z*. From the MS scan, the 10 most abundant peptide ions were selected for fragmentation via HCD with a normalized collision energy of 27, an isolation window of 1.6 *m/z*, and a dynamic exclusion of 30 s. MS/MS spectra were recorded at a resolution of 15,000 with an AGC target of $1e^5$ and a maximum injection time of 50 ms. Unassigned charges, as well as charges of +1 and >+8 were excluded from precursor selection.

2.3 | Data processing and label-free quantification

Proteome Discoverer 2.4 software (version 2.4.1.15; Thermo Fisher Scientific, Dreieich, Germany) was used for peptide and protein identification via database search (Sequest HT search engine) against Ensembl pig protein database (version 11.1, http://www.ensembl.org); considering full tryptic specificity, allowing for one missed tryptic cleavage site, with precursor mass tolerance 10 ppm, and fragment mass tolerance 0.02 Da. Carbamidomethylation of Cys was set as a static modification. Dynamic modifications included deamidation of Asn, Gln, and Arg, oxidation of Pro and Met; and a combination of Met loss with acetylation on protein N-terminus. Percolator [10] was used for validating peptide spectrum matches and peptides, accepting only the top-scoring hit for each spectrum, and satisfying the cutoff values for FDR < 1%, and posterior error probability < 0.01. The final list of proteins adhered to the strict parsimony principle.

Quantification of proteins, after precursor recalibration, was based on summed intensity values (at RT apex) for all unique peptides per protein. Peptide abundance values underwent normalization based on the total peptide amount. Protein ratios were then computed using the pairwise ratio-based approach, with a background-based Student's *t*-test as the hypothesis test [6], yielding ratios, and corresponding significance values for the individual proteins. *P*-values underwent adjustment for multiple testing via Benjamini–Hochberg correction. Proteins with an adjusted *p*-value < 0.05 were considered significant.

2.4 | Data analysis of porcine vitreous proteome via Gene Set Enrichment Analysis Tool

The entire proteome dataset from porcine vitreous was analyzed with the Gene Set Enrichment Analysis Tool (GSEA v4.3.2, https://www.gsea-msigdb.org/gsea/index.jsp) [11, 12] using the human hallmark gene set collection from the Molecular Signatures Database (MSigDB v2023.2.Hs), which comprises 50 gene sets in total [11, 13, 14]. GSEA is a computational method that evaluates whether a predefined set of genes exhibits statistically significant, consistent differences between two phenotypes [11, 12]. The 50 available hallmark gene sets represent specific well-defined biological processes and display coherent expression [11, 13, 14]. To exclude very small gene sets (<15 genes) that may be prone to noise, or very large gene sets (<500 genes) that may lack specificity, a gene set size filter was applied, leaving 30 hallmark gene sets for further analysis (Table S2). Human orthologue gene names were used for GSEA analysis. In cases where proteins were not identified in all 22 samples, missing normalized abundance values were imputed. Venn diagrams were generated using the open-source tool http://bioinformatics.psb.ugent.be/webtools/Venn/. Protein interaction analysis was conducted using the String database (version 12, https://string-db.org/). Cnetplots from GSEA analysis results were created in R (version 4.3.1; R Core Team (2023), Vienna, Austria, https://www.R-project.org/) [15] with the packages "clusterprofiler" (version 4.10.1) [16] and "enrichplot" (version 1.22.0) [17].

3 | RESULTS

3.1 | The porcine vitreous comprises 1404 different proteins, with 19% exhibiting differential abundance ratios in the diabetic state

With differential proteomics we detected 1490 identifications, representing a total of 1404 different proteins in porcine vitreous (Table S1). Of these proteins, 1270 were identified in both groups, whereas 10 proteins were only identified in the wt group and 124 proteins were exclusively identified in the *INS*^{C94Y} group (Figure 1A). Quantitative analysis showed significant (adjusted *p*-value < 0.05) abundance ratio differences between groups for 266 proteins, representing abundance ratio changes for 19% of the vitreous proteome. From these differentially abundant proteins, 27 were lower abundant and 239 were higher abundant in *INS*^{C94Y} vitreous (Figure 1B). To identify proteins of interest with robust abundance differences, an additional stringent coverage threshold for protein identification (minimum identification in 6/11 samples per group) was applied, resulting in 73 differentially abundant proteins. Of these, 67 were significantly higher abundant in *INS*^{C94Y} vitreous, while six exhibited lower abundance (Figure 1C).

3.2 | Integrin beta 1, Cytochrome c oxidase subunit 2, and GRIFIN are highly abundant in the vitreous of *INS*^{C94Y} pigs

Since we were especially interested in proteins which were exclusively identified in vitreous from the *INS*^{C94Y} pig, we screened for possible proteins of interest among the 73 differentially abundant identifications.

Integrin beta 1 (ITGB1), a multifunctional molecule with a vital role in cell-matrix interactions and close association with the retinal internal limiting membrane [18], was identified with a coverage of 9/11 in *INS*^{C94Y} vitreous, whereas it was not identified in any of the vitreous samples of wt pigs (Table 1). Similarly, cytochrome c oxidase subunit 2 (MT-CO2 or COX2), a subunit of cytochrome c oxidase, which is the terminal enzyme complex of the mitochondrial respiratory chain [19], was identified with a high coverage in *INS*^{C94Y} vitreous (8/10) but was not detected in wt vitreous (Table 1).

Among the proteins with the best coverage in *INS*^{C94Y} vitreous samples (11/11), Galectin-Related Inter-Fiber Protein (GRIFIN) showed the highest abundance ratio (*INS*^{C94Y}/wt: 10) with strong significance (adj. *p* value 2.1E − 08) (Table 2). GRIFIN is a member of the family of adhesion/growth-regulatory galectins which was first described in lens fibers of rats [20] but is also comprehensively described in lenses of birds and zebrafish [21, 22]. Interestingly, this protein was recently also identified in the vitreous of 8-week-old C57BL/6 mice with induced diabetes [23]. However, the exact role of this protein in diabetes-induced eye lesions has not yet been elucidated.

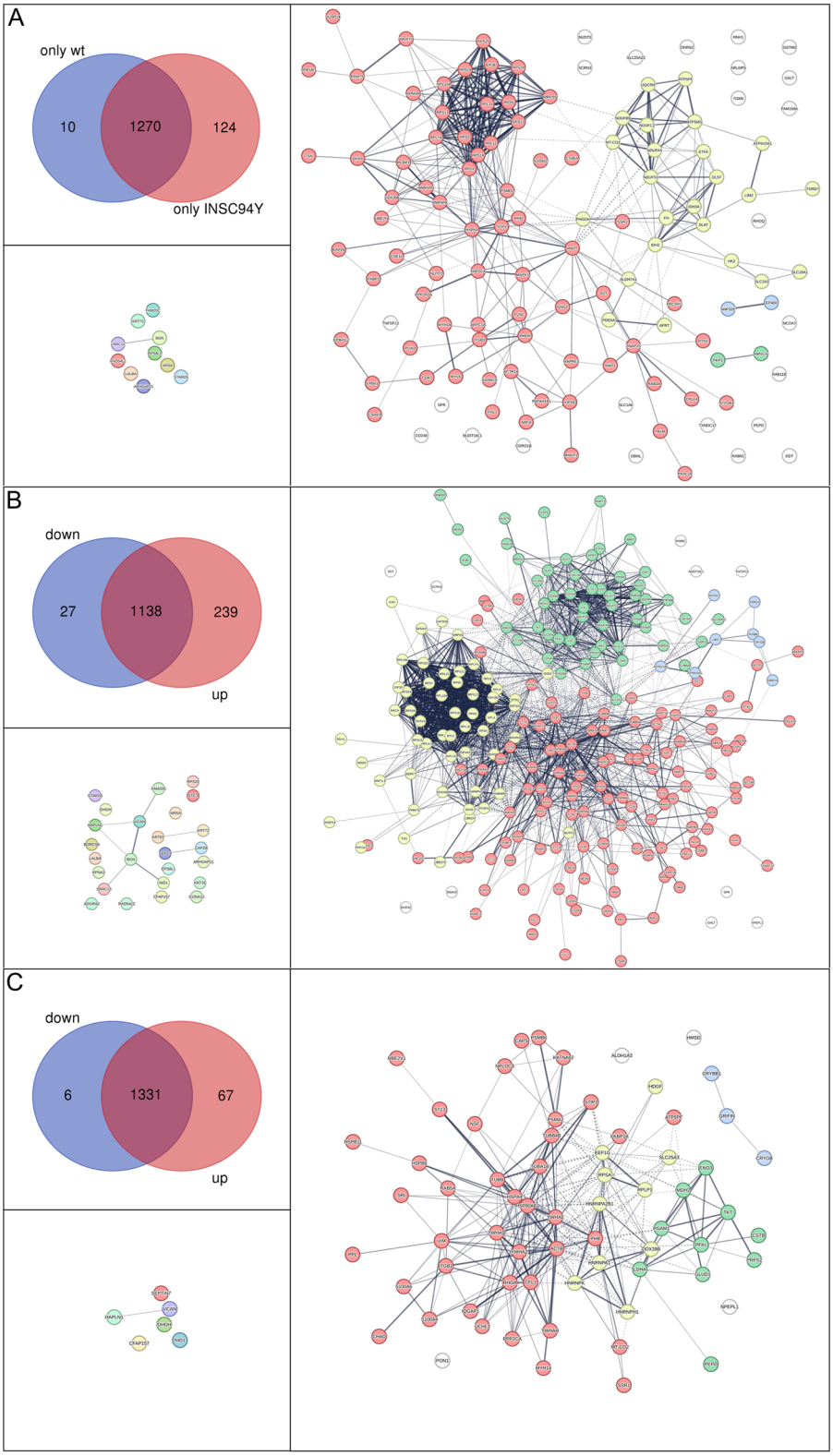

FIGURE 1 All proteins from porcine vitreous were identified with mass spectrometric analysis. (A) Proteins only detected in one group, (B) proteins with significantly changed abundance between groups and (C) proteins with significantly changed abundance and a minimum identification rate of 6/11 samples. Venn diagrams (top left panels) show the amount of identified proteins in the porcine vitreous as well as (A) the amount of proteins only identified in one group (adj.$p < 0.05$, blue: wt; red: INS^{C94Y}), and (B), (C) amount of differentially abundant proteins (adj.$p < 0.05$, blue: down in INS^{C94Y}, red: up in INS^{C94Y}). Respective proteins are shown in STRING networks: (A) lower left panel: wt, right panel: INS^{C94Y}, (B)+F(C) lower left panels: down in INS^{C94Y}, right panels: up in INS^{C94Y}. kmeans clustering was performed to sort interaction networks with >30 proteins into four distinct clusters.

TABLE 1 High coverage proteins (detected in min 6/11 samples) only identified in *INS*^{C94Y} vitreous.

Gene name[a]	Description[b]	Abundance ratio: (*INS*^{C94Y})/(wt) [c]	Abundance ratio adj. *p*-value: (*INS*^{C94Y})/(wt) [d]	Peaks found in (*INS*^{C94Y})[e]	Peaks found in (wt)[f]
PEPD	Uncharacterized protein	100.00	8.8373E – 17	9	0
SSR1	Signal sequence receptor, alpha	100.00	8.8373E – 17	9	0
ITGB1	Integrin, beta 1	100.00	8.8373E – 17	9	0
MT-CO2	Cytochrome c oxidase subunit 2	100.00	8.8373E – 17	8	0
PPP2CA	Serine/threonine-protein phosphatase	100.00	8.8373E – 17	8	0
DDX39B	DEAD (Asp-Glu-Ala-Asp) box polypeptide 39B	100.00	8.8373E – 17	8	0
MYH14	Myosin, heavy chain 14, non muscle	100.00	8.8373E – 17	7	0
IQGAP1	IQ motif containing GTPase activating protein 1	100.00	8.8373E – 17	6	0
ATP5J	ATP synthase-coupling factor 6, mitochondrial	100.00	8.8373E – 17	6	0
RHOA	ras homolog family member A	100.00	8.8373E – 17	6	0
HNRNPK	Heterogeneous nuclear ribonucleoprotein K	100.00	8.8373E – 17	6	0
HSPA4	Heat shock 70 kDa protein 4	100.00	8.8373E – 17	6	0

[a]Gene name.
[b]Protein description.
[c]Ratio of protein abundance differences in *INS*^{C94Y} compared to wt.
[d]Statistical significance of protein abundance differences following FDR *p*-value adjustment.
[e]Number of samples in which peaks were found in *INS*^{C94Y}.
[f]Number of samples in which peaks were found in wt.

3.3 | Functional insights from proteomic analysis of enriched protein networks point to increased metabolic processes, vascular dysregulation, and autophagy in diabetic eyes

To elucidate the functional implications of protein abundance variations in diabetic vitreous, GSEA was conducted (Table S2). Three gene sets were significantly enriched in vitreous from wt pigs (Table 3). The gene set with the most significant enrichment score was epithelial–mesenchymal transition, followed by coagulation and KRAS signaling (Table 3 and Figure 2A–C). These biological processes may be part of the physiological function of the vitreous and may consequently be impaired in the diseased state. In diabetic vitreous, on the other hand, five gene sets showed significant enrichment scores (Table 4), pointing to the role of these processes in diabetes-associated pathological changes in ocular tissues. The most significantly enriched gene set was MYC targets, followed by oxidative phosphorylation, fatty acid metabolism, mTORC1 signaling, and unfolded protein response (UPR) (Table 3 and Figure 3D–H).

The gene set UPR describes genes involved in a cellular stress response related to the endoplasmic reticulum (ER) [24]. Sixteen identifications from our vitreous data were assigned to this gene set, of which 10 were core enriched, meaning these proteins associated to the leading-edge subset, contributing most to the enrichment results (Figure 2D).

Fifty-five identifications were included in the oxidative phosphorylation gene set, of which 47 were core enriched (Figure 2E), and 34 identifications from our dataset were allocated to the gene set fatty acid metabolism, of which 27 were core enriched (Figure 2F). Both fatty acid metabolism and oxidative phosphorylation are metabolic processes that contribute to the generation of energy in the form of ATP [25] and appear to be altered by chronic hyperglycemia in the *INS*^{C94Y} diabetic pig model. Six proteins from our vitreous proteome input were present in both gene sets (Figure 3A). These overlapping proteins were all mitochondrial enzymes (LDHA, MDH1, MDH2, ECHS1, SUCLA2, and DLST). Most of these enzymes play a role in the energy generation via the citric acid cycle thereby regulating cellular metabolism, pointing to dysregulated metabolic processes in ocular tissue under chronic hyperglycemia.

A total of 49 protein identifications were allocated to the mTORC1 signaling gene set, of which 32 were core enriched (Figure 2G), indicating that the corresponding genes are upregulated through activation of the mTORC1 complex. Activation of the mTORC1 complex has been described as a dysregulated process in DR in mice, especially in connection with the autophagy of retinal cells [26]. The gene set MYC targets contains genes that are regulated by the transcription factor MYC, which promotes sprouting angiogenesis in the eyes of mice with DR [27, 28]. From our data input, 56 genes were allocated to the MYC targets gene set, of which 37 were core enriched (Figure 2H). The intersection of MYC and mTORC1 signaling pathways involves

TABLE 2 Proteins which were only identified in all *INS*^{C94Y} vitreous samples (detected in 11/11 *INS*^{C94Y} samples).

Gene name[a]	Description[b]	Abundance ratio: (*INS*^{C94Y})/(wt)[c]	Abundance ratio adj. *p*-value: (*INS*^{C94Y})/(wt)[d]	Peaks found in (*INS*^{C94Y})[e]	Peaks found in (wt)[f]
GRIFIN	Galectin-Related Inter-Fiber Protein	10.03	0.0000	11	11
S100A4	S100 calcium binding protein A4	7.10	0.0000	11	10
S100A6	S100 calcium binding protein A6	5.45	0.0001	11	11
TUBA1B	Tubulin alpha-1B chain	4.50	0.0010	11	11
YWHAZ	Uncharacterized protein	4.41	0.0012	11	11
TKT	Transketolase	3.72	0.0061	11	9
TUBB	Tubulin, beta 2A	3.64	0.0074	11	9
HSP90AB1	Heat shock 90 kD protein 1, beta	3.26	0.0189	11	11
PGAM1	Phosphogycerate mutase 1 (brain)	3.10	0.0277	11	11
VIM	Vimentin	3.07	0.0296	11	11
LDHA	Lactate dehydrogenase A	3.07	0.0299	11	11
MDH2	Malate dehydrogenase 2, NAD (mitochondrial)	3.03	0.0335	11	7
YWHAE	Uncharacterized protein	3.00	0.0360	11	11
CRYBB1	Crystallin, beta B1	2.99	0.0365	11	11
PHB	Uncharacterized protein	2.98	0.0369	11	5
ENO3	Enolase 3 (beta, muscle)	2.90	0.0453	11	11
RPSA	Uncharacterized protein	2.87	0.0485	11	9
HAPLN1	Hyaluronan and proteoglycan link protein 1	0.31	0.0039	11	11

[a]Gene name.
[b]Protein description.
[c]Ratio of protein abundance differences in *INS*^{C94Y} compared to wt.
[d]Statistical significance of protein abundance differences following FDR *p*-value adjustment.
[e]Number of samples in which peaks were found in *INS*^{C94Y}.
[f]Number of samples in which peaks were found in wt.

reciprocal regulation of their activities at various points [29]. Since shared proteins in these pathways may be interesting targets for diagnostics and therapy, we were interested in analyzing the overlap between MYC and mTORC1 leading-edge subsets. We observed an overlap of seven identifications allocated to both gene sets, which clustered to the proteasome subunit (PSMA4), the heat shock protein family (HSPE1, HSPD1), and proteins with enzyme activity (PPIA, PGK1, HPRT1, LDHA) (Figure 3B).

4 | DISCUSSION

Understanding the intricate pathophysiological mechanisms underlying DR and diabetic cataracts, both consequences of chronic hyperglycemia, is crucial for developing effective treatments. While various models like Akita *Ins2*$^{+/C96Y}$ [30] and Munich *Ins2*$^{+/C95S}$ [31] mutant mice are valuable for diabetes research, their translational relevance can be limited due to significant differences in several features such as size, metabolism, and a much shorter life-span, which impedes investigations on the effects of long-term chronic hyperglycemia over an extended period of time. Pigs offer a compelling alternative due to their anatomical, physiological, and metabolic similarities to humans [32], making them ideal for biomedical research. In particular, *INS*^{C94Y} pigs present a promising large animal model, mimicking several diabetes-related features observed in humans [32]. These pigs express a mutant form of insulin resulting in a stable diabetic phenotype early after birth, rapidly progressing into chronic hyperglycemia [6]. This long-term exposure to elevated blood glucose levels induces severe damage to nerves and blood vessels, affecting several organs including the eye [5]. Severe ocular lesions include extraretinal hemorrhages and cotton-wool spots as well as retinal edema near the optic nerve [4], which are all hallmarks of DR in humans and, to our knowledge, are not observed together in other animal models for diabetes mellitus. Further, *INS*^{C94Y} pigs are a good model to study diabetes-induced lens cataracts, since cataract formation starts as early as 8 days after birth and mature cataract is fully developed by the age of 4.5 months [4, 6]. The intentionally suboptimal insulin treatment regimen of these pigs establishes moderate hyperglycemia [5, 8], enabling longevity despite diabetic complications and thus allowing long-term investigations of DR and cataract pathophysiology—a major advantage compared to short-lived rodent diabetes models.

TABLE 3 Significantly enriched gene sets correlating to wt group.

Hallmark gene set name[a]	Size[b]	NES[c]	NOM *p*-val[d]	FDR *q*-val[e]	Rank at max[f]	Leading edge[g]	Enriched genes (leading edge depicted in bold)[h]
EPITHELIAL_MESENCHYMAL_TRANSITION	83	−2.23	0.0000	0.0016	287	Tags = 45%, list = 21%, signal = 53%	**ITGB1 FBLN5 COMP CD59 VIM BASP1 COL6A2 ENO2 FN1 PPIB LGALS1 TPM2 TGM2 FUCA1 ANPEP SERPINE1 PLOD2 GPC1 QSOX1 SPOCK1 NTM CD44 PDGFRB CALU ECM1 SDC4 NOTCH2 PFN2 CTHRC1 PLOD1 IGFBP3 LOXL1 SPP1 HTRA1 IGFBP2 CDH2 IGFBP4 COL4A2 TGFBI LRP1 COL1A2 PTX3 TIMP3 CDH11 MMP2 BMP1 FMOD COL5A2 COL5A1 APLP1 COL3A1 CXCL12 COL11A1 ECM2 LRRC15 FBN1 THBS1 FBLN1 SPARC TFPI2 MXRA5 TNC CDH6 SCG2 PCOLCE THY1 VCAN FBLN2 COL5A3 BGN TIMP1 LUM EFEMP2 COL4A1 LAMC1 SFRP1 ABI3BP VCAM1 SLIT2 WNT5A COL16A1 NID2 SERPINE2**
COAGULATION	60	−2.11	0.0000	0.0029	256	Tags = 43%, list = 19%, signal = 51%	**F9 COMP GNB2 CAPN2 DUSP14 FN1 ANXA1 ARF4 CSRP1 SERPINE1 PRSS23 VWF FGG A2M C8G APOA1 LAMP2 LGMN CFB SERPING1 CLU SERPINC1 THBD C3 HTRA1 FGA C1R LRP1 C2 F8 TIMP3 MMP2 BMP1 F2 CFI C1QA PLG CPB2 PROC C9 ITIH1 CFH FBN1 CTSH HRG THBS1 C8A SPARC F10 TFPI2 SERPINA1 CFD F12 TF CPQ ADAM9 TIMP1 PROS1 CTSO CTSB**
KRAS_SIGNALING_UP	29	−1.76	0.0116	0.0373	229	Tags = 41%, list = 17%, signal = 49%	**CA2 SNAP25 ADAM17 ACE ALDH1A3 FUCA1 LCP1 JUP SNAP91 SPARCL1 ARG1 CFB IGFBP3 SPP1 SCG5 ADGRA2 CSF2RA CFH CPE EPHB2 RELN SCG3 SERPINA3 CTSS RBP4 APOD PCSK1N WNT7A SPON1**

Note: Gene names comprising the leading edge subset are depicted in bold.
[a]Hallmark gene set name as described in the GSEA tool.
[b]Number of genes in the gene set after filtering out those genes not in the vitreous dataset.
[c]Normalized enrichment score.
[d]Nominal *p*-value describing the statistical significance of the enrichment score.
[e]False discovery rate.
[f]Position in the ranked GSEA gene list at which the maximum enrichment score occurred.
[g]The three statistics used to define the leading edge subset of each single gene set.
[h]Genes enriched in the respective hallmark gene sets.

Our comprehensive analysis of the porcine vitreous identified 1404 proteins, of which 19% were differentially abundant in the diabetic phenotype, shedding light on the molecular processes occurring in adjacent ocular tissues affected by diabetes. While similar studies have been conducted on the vitreous of mice and humans [23, 33], the porcine vitreous proteome has not been described previously, neither in health nor in disease. Interestingly, we identified several proteins that were only detected in the diabetic phenotype and were not present in the vitreous of wt controls, indicating a possible role in disease pathogenesis. One of these proteins, ITGB1, has previously been described in the eyes of C57BL/6J mice with induced diabetes, where retinal capillary pericytes increased its expression under high glucose conditions in early DR, promoting angiogenesis [34]. This pro-angiogenic role of ITGB1 is based on the fact that integrins act as ligands for various angiogenic factors [35]. Since sprouting angiogenesis is one of the hallmarks of DR, ITGB1 has been described as a potential target for new treatment options [36]. Similarly, elevated levels of COX2 in our dataset point to ongoing vascular sprouting under hyperglycemic conditions, which is in line with previous studies in different mouse models for proliferative DR, describing COX2 as a mechanistic link between angiogenesis and inflammation in the pathogenesis of DR [37, 38]. Moreover, increased COX2 expression has also been reported in rat lens epithelial cells exposed to a high glucose environment [39]. To our knowledge, ITGB1 and COX2 have not been described as proteins of vitreal origin, therefore the abundances of ITGB1 and COX2 in *INS*^{C94Y} vitreous most likely originate from the retina or the lens, underlining the importance of the vitreous as a reservoir for potential biomarkers in DR. Future studies need to

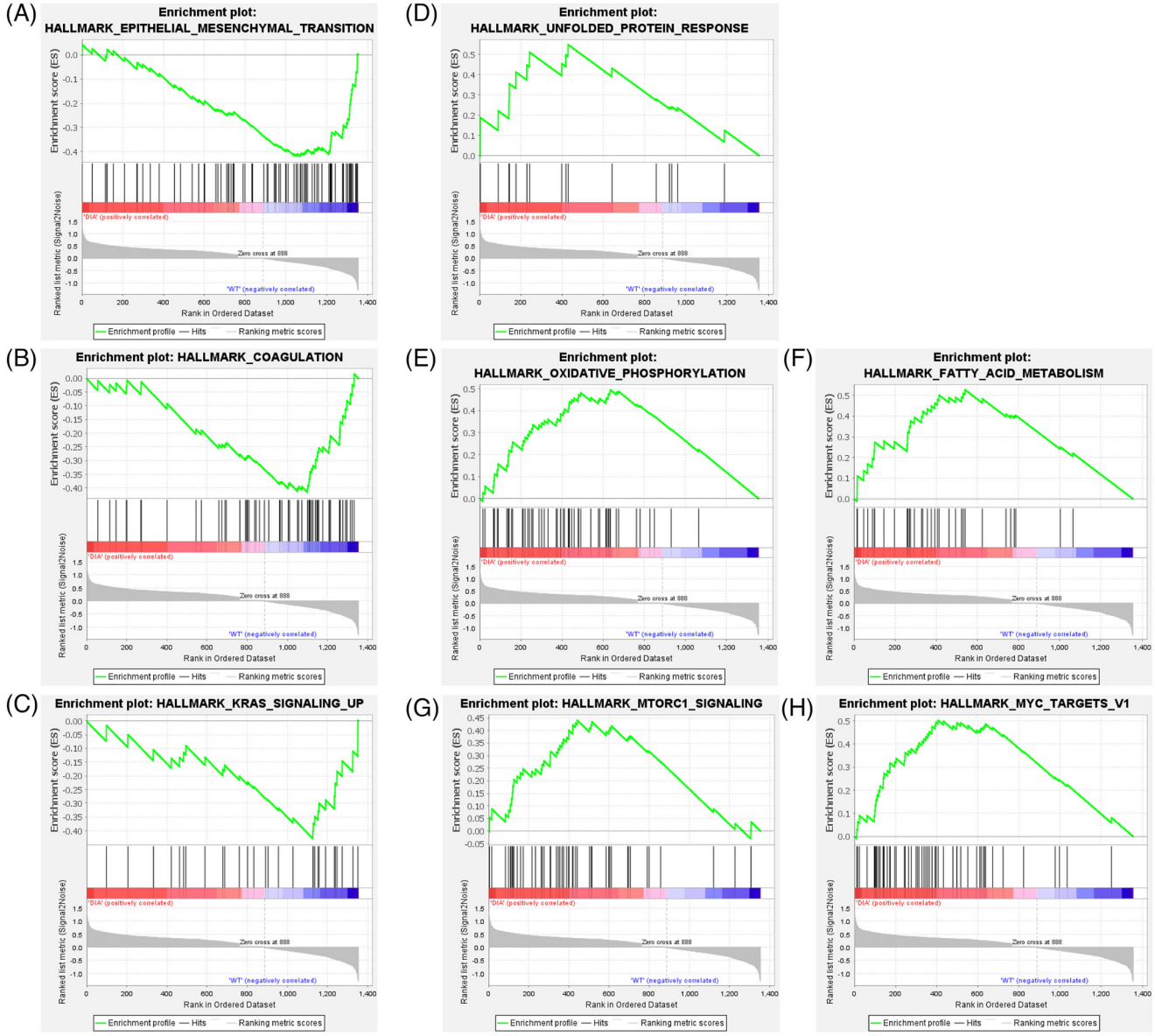

FIGURE 2 GSEA enrichment plots for all significantly enriched hallmark gene sets obtained from the vitreous input data. (A)–(C) enrichment correlating to wt group, (D)–(H) enrichment correlating to *INS*^{C94Y} group. The graphical view of the enrichment scores shows the enrichment score correlating to each gene set (A–C: lowest point, D–H: highest point of the green graph), the leading edge subset (all ranked genes leading up to respective enrichment score), the appearance of the members of the gene set in the ranked list of genes (each line represents a gene) and the ranking metrics that measure a gene's correlation with a group (red: correlation with *INS*^{C94Y}, blue: correlation with wt phenotype).

determine the origin of these molecules and their suitability for reliable diagnosis and stratification, or as biomarkers for the prognosis of ocular pathology in diabetes mellitus.

GRIFIN, a protein related to the galectin family [40], was identified in both groups but was significantly higher abundant in *INS*^{C94Y} vitreous. Similar to our findings, GRIFIN has previously been described with significantly increased abundance in vitreous of 8-week-old C57BL/6 mice with induced diabetes [23]. Allocated to the lens, mammalian GRIFIN has lost its lectin activity, and therefore its capacity to bind carbohydrates [22]. Instead, it has been assumed to play a role in maintaining lens transparency due to strong interaction with the main structural lens components—crystallins [40, 41]. In fact, mammalian GRIFIN has been presumed to function as a crystallin rather than a galectin [22]. GRIFIN, therefore, presents an intriguing avenue for further exploration, especially regarding diabetes-associated complications in the eye such as cataracts.

Our approach of analyzing the entire vitreous, including regions adjacent to the retina, lens, and ciliary body, provides a holistic view of diabetes-induced molecular mechanisms in eye tissues. GSEA allowed us to further explore the vitreous proteomics data and investigate its relevance in ocular manifestation of diabetes mellitus.

Among the gene sets identified through GSEA, the UPR pathway was enriched in diabetic vitreous. The UPR is regulatory mechanism, which is activated in response to unfolded or misfolded proteins

TABLE 4 Significantly enriched gene sets correlating to *INS*^{C94Y} group.

Hallmark gene set name[a]	Size[b]	NES[c]	NOM *p*-val	FDR *q*-val[d]	Rank at max[e]	Leading edge[f]	Enriched genes (leading edge depicted in bold)[g]
MYC_TARGETS_V1	56	2.18	0.0000	0.0094	407	Tags = 66%, list = 30%, signal = 91%	**PHB1 LDHA YWHAE YWHAQ CCT2 PGK1 TCP1 HDGF HSP90AB1 HPRT1 HNRNPD PRDX3 HNRNPA2B1 NPM1 VDAC3 CCT5 HNRNPA1 SRSF2 NAP1L1 EIF4A1 RPL18 PRPS2 RAN HSPE1 PSMA2 PPIA COX5A APEX1 HSPD1 PSMA4 EEF1B2 GLO1 PHB2 PCBP1 TUFM RPS3 KPNB1 CANX SLC25A3 RPL14 HNRNPA3 RPS5 EIF3D RPS10 RPS6 VDAC1 GOT2 CYC1 PSMA6 NME1 RPL6 RACK1 CCT3 CCT4 SET PA2G4**
OXIDATIVE_ PHOSPHORYLATION	55	2.17	0.0000	0.0047	635	Tags = 85%, list = 47%, signal = 154%	**LDHA ATP5PF DLST IDH2 OGDH PDHX MDH2 UQCRC1 SLC25A4 PRDX3 HSPA9 CYB5R3 VDAC3 SLC25A5 NDUFC2 IDH3A GPI GLUD1 CYB5A MDH1 LDHB COX5B COX5A VDAC2 OAT PHB2 ECHS1 NDUFA4 PDHB UQCRH ETFA DLAT CS COX6B1 NDUFS3 SLC25A3 NDUFA5 AIFM1 FH NDUFS1 SLC25A11 COX4I1 VDAC1 SUCLA2 GOT2 CYC1 RHOT1 UQCRC2 ACAT1 DLD SDHA CYCS NDUFV1 ATP1B1 ACO2**
FATTY_ ACID_METABOLISM	34	2.03	0.0000	0.0012	540	Tags = 79%, list = 40%, signal = 129%	**LDHA AOC3 MIF DLST MDH2 CA2 HSP90AA1 GLUL YWHAH MDH1 ERP29 ME1 ENO2 EPHX1 PRDX6 APEX1 LGALS1 ACSM3 ENO3 ECHS1 PDHB FASN ALDH1A1 CRYZ GAPDHS CBR3 FH SUCLA2 GPD1 DLD SDHA MGLL PTPRG ACO2**
MTORC1_SIGNALING	49	1.89	0.0000	0.0050	442	Tags = 65%, list = 33%, signal = 93%	**SSR1 LDHA PFKL PGK1 PSMA3 RAB1A HPRT1 TUBA4A STIP1 HSPA9 HSPA4 PPA1 HK2 GPI ME1 ENO1 HSPE1 PPIA PGM1 PSMD12 HSPD1 PSMA4 PSMB5 GAPDH TPI1 PRDX1 HSPA5 ACTR3 HSP90B1 PHGDH CANX SLC2A3 SLC2A1 CFP FKBP2 GCLC PLOD2 VLDLR UBE2D3 NAMPT GOT1 PNP LDLR LGMN CALR IGFBP5 GLA STC1 IFI30**
UNFOLDED_ PROTEIN_RESPONSE	16	1.72	0.0076	0.0229	430	Tags = 63%, list = 32%, signal = 90%	**SSR1 YWHAZ HSPA9 NPM1 EEF2 KIF5B EIF4A1 HSPA5 HSP90B1 PDIA6 EIF4A2 CALR DNAJC3 HYOU1 STC2 EDC4**

Note: Gene names comprising the leading edge subset are depicted in bold.
[a]Hallmark gene set name as described in the GSEA tool.
[b]Number of genes in the gene set after filtering out those genes not in the vitreous dataset.
[c]Normalized enrichment score.
[d]Nominal *p*-value describing the statistical significance of the enrichment score.
[e]False discovery rate.
[f]Position in the ranked GSEA gene list at which the maximum enrichment score occurred.
[g]The three statistics used to define the leading edge subset of each single gene set.
[h]Genes enriched in the respective hallmark gene sets.

occurring due to ER stress (reviewed in Hetz et al. [42]). The identification of UPR-associated proteins in diabetic vitreous may therefore indicate the presence of ER stress in the adjacent tissues, such as the retina and the lens. As shown in lenses of galactosemic rats, ER stress-induced prolonged UPR activation can provoke lens cell apoptosis and lens opacity [43], an observation which may also apply to the cataract formation in the *INS*^{C94Y} pigs used in our study. In the retina of ApoE$^{-/-}$:Ins2$^{+/Akita}$ mice, chronic ER stress can be triggered by persistent hyperglycemia [44] and subsequent, prolonged UPR activation can cause severe damage through neurodegenerative, proinflammatory,

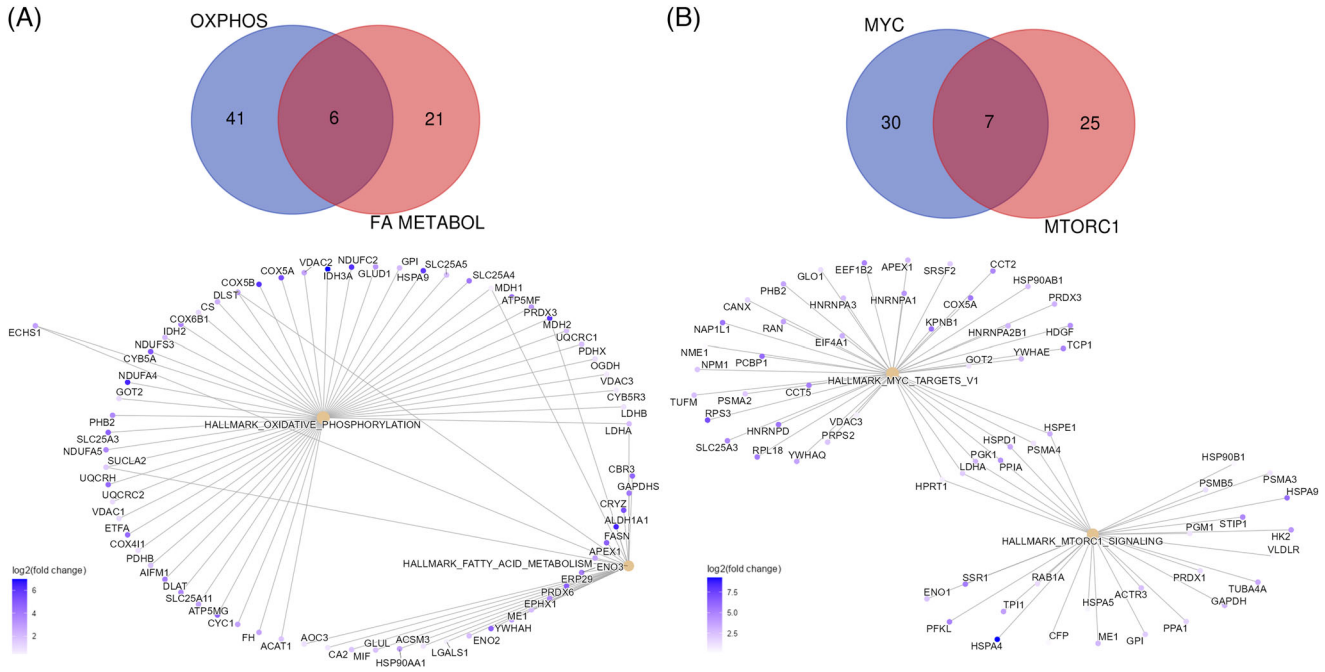

FIGURE 3 Venn diagram (top) and Cnetplot (bottom) showing overlap of proteins allocated to (A) oxidative phosphorylation and fatty acid metabolism with overlapping proteins LDHA, MDH1, MDH2, ECHS1, SUCLA2 and DLST and (B) MYC targets and mTORC1 pathway with overlapping proteins PSMA4, HSPE1, HSPD1, PPIA, LDHA, PGK and HPRT1.

and proapoptotic signaling, which was shown in retinal Mueller cells from rats and human retinal organoids [45, 46]. Similar processes may also occur in the retina of *INS*^{C94Y} pigs, indicating a role of this pathway in the development of severe long-term hyperglycemia-induced ocular complications in this model, which merits further investigations.

The enrichment of oxidative phosphorylation and fatty acid metabolism pathways in our vitreous protein dataset points to dysregulated glucose and lipid metabolism in the eyes of individuals with diabetes. As shown in multiple studies on rodent diabetes models and human diabetic retinas, this dysregulation likely contributes to the pathogenesis of DR through mitochondrial dysfunction, increased vascularization, and neurodegeneration of the retina [47–50]. Especially proteins from our porcine vitreous dataset allocated to both pathways are interesting for understanding the molecular mechanisms driving the development of DR and may disclose possible targets for therapeutic interventions in hyperglycemia-induced dysregulated metabolism.

Analysis further revealed a clustering of proteins related to the mTORC1 pathway in *INS*^{C94Y} vitreous. The mTORC1 complex has previously been described as dysregulated in DR in mice, especially in connection with autophagy of retinal cells [26]. Since low glucose levels have been shown to suppress mTORC1 signaling [51], thereby increasing autophagy [26], the enriched mTORC1 pathway in combination with high glucose levels in *INS*^{C94Y} vitreous point to decreased autophagy in porcine diabetic eyes. This has detrimental effects on cellular homeostasis in the retina [52], highlighting the importance of further elucidating the role of mTORC1-induced autophagy in disease progression.

The most enriched gene set from vitreous protein data was associated with the transcription factor MYC, which is implicated in diabetes-induced ocular pathologies. Increased MYC activity has been described in correlation with diabetes-induced elevated glucose levels in retinal Mueller cells of rats and retinas of mice, promoting the release of pro-inflammatory cytokines and neovascularization in the retina [1, 27, 28, 53]. In the vitreous, however, MYC activity has not been previously described. The enrichment of MYC targets in *INS*^{C94Y} vitreous underscores the model's relevance in studying angiogenic processes associated with DR.

Several of the vitreous proteins enriched in the mTORC1 and MYC gene set were present in both pathways. Since the ocular manifestation of diabetes-induced lesions in the eye is not characterized by a singular pathway but involves interconnected communication across numerous signaling pathways, these overlapping proteins may be useful to simultaneously target multiple key pathways for diagnostics and therapy.

In conclusion, our study is the first to describe the porcine vitreous proteome and unveil differences associated with chronic hyperglycemia. The identification of ITGB1 and COX2 in the vitreous of *INS*^{C94Y} transgenic pigs underlines the importance of this tissue as a reservoir for potential biomarkers for DR and the increased abundance of GRIFN may further elucidate molecular mechanisms in diabetes-induced cataract formation. Moreover, the enrichment of gene sets MYC and mTOR1 with implications in increased neovascularization and reduced autophagy, provide valuable insights into the pathophysiological processes underlying long-term hyperglycemia-induced eye complications. Further investigation into the role of vitreal

proteins in diabetic ocular pathologies is essential for advancing our understanding and developing targeted therapies.

ACKNOWLEDGMENTS

The authors thank Barbara Amann, Sieglinde Hirmer, and Tanja Weißer for critical discussions and excellent technical assistance. This work was supported by Deutsche Forschungsgemeinschaft in the SPP 2127, Grant Number DFG DE 719/7-1 (to C.A.D) and the German Center for Diabetes Research (DZD), Grant 82DZD08D03SPP (to E.W.).

Open access funding enabled and organized by Projekt DEAL.

CONFLICT OF INTEREST STATEMENT

The authors declare no conflicts of interest.

DATA AVAILABILITY STATEMENT

The mass spectrometry proteomics data have been deposited to the ProteomeXchange Consortium via the PRIDE [54] partner repository (https://www.ebi.ac.uk/pride/archive) with the dataset identifier PXD038198.

ORCID

Cornelia A. Deeg https://orcid.org/0000-0003-0375-3190

REFERENCES

1. Yao, X., Xue, Y., Ma, Q., Bai, Y., Jia, P., Zhang, Y., Lai, B., He, S., Ma, Q., Zhang, J., Tian, H., Yin, Q., Zheng, X., & Zheng, X. (2023). 221S-1a inhibits endothelial proliferation in pathological angiogenesis through ERK/c-Myc signaling. *European Journal of Pharmacology*, *952*, 175805. https://doi.org/10.1016/j.ejphar.2023.175805
2. Balaiya, S., Zhou, Z., & Chalam, K. V. (2017). Characterization of vitreous and aqueous proteome in humans with proliferative diabetic retinopathy and its clinical correlation, *Proteomics Insights*, *8*, 1178641816686078. https://doi.org/10.1177/1178641816686078
3. Forbes, J. M., & Cooper, M. E. (2013). Mechanisms of diabetic complications. *Physiological Reviews*, *93*, 137–188. https://doi.org/10.1152/physrev.00045.2011
4. Kleinwort, K. J. H., Amann, B., Hauck, S. M., Hirmer, S., Blutke, A., Renner, S., Uhl, P. B., Lutterberg, K., Sekundo, W., Wolf, E., & Deeg, C. A. (2017). Retinopathy with central oedema in an INS C94Y transgenic pig model of long-term diabetes. *Diabetologia*, *60*, 1541–1549. https://doi.org/10.1007/s00125-017-4290-7
5. Renner, S., Blutke, A., Clauss, S., Deeg, C. A., Kemter, E., Merkus, D., Wanke, R., & Wolf, E. (2020). Porcine models for studying complications and organ crosstalk in diabetes mellitus. *Cell and Tissue Research*, *380*, 341–378. https://doi.org/10.1007/s00441-019-03158-9
6. Renner, S., Braun-Reichhart, C., Blutke, A., Herbach, N., Emrich, D., Streckel, E., Wünsch, A., Kessler, B., Kurome, M., Bähr, A., Klymiuk, N., Krebs, S., Puk, O., Nagashima, H., Graw, J., Blum, H., Wanke, R., & Wolf, E. (2013). Permanent neonatal diabetes in INS C94Y transgenic pigs. *Diabetes*, *62*, 1505–1511. https://doi.org/10.2337/db12-1065
7. Wolf, E., Braun-Reichhart, C., Streckel, E., & Renner, S. (2014). Genetically engineered pig models for diabetes research. *Transgenic Research*, *23*, 27–38. https://doi.org/10.1007/s11248-013-9755-y
8. Blutke, A., Renner, S., Flenkenthaler, F., Backman, M., Haesner, S., Kemter, E., Ländström, E., Braun-Reichhart, C., Albl, B., Streckel, E., Rathkolb, B., Prehn, C., Palladini, A., Grzybek, M., Krebs, S., Bauersachs, S., Bähr, A., Brühschwein, A., Deeg, C. A., … Wolf, E. (2017). The Munich MIDY Pig Biobank—a unique resource for studying organ crosstalk in diabetes. *Molecular Metabolism*, *6*, 931–940. https://doi.org/10.1016/j.molmet.2017.06.004
9. Grosche, A., Hauser, A., Lepper, M. F., Mayo, R., Von Toerne, C., Merl-Pham, J., & Hauck, S. M. (2016). The proteome of native adult Müller glial cells from murine retina. *Molecular & Cellular Proteomics: MCP*, *15*, 462–480. https://doi.org/10.1074/mcp.M115.052183
10. Käll, L., Canterbury, J. D., Weston, J., Noble, W. S., & Maccoss, M. J. (2007). Semi-supervised learning for peptide identification from shotgun proteomics datasets. *Nature Methods*, *4*, 923–925. https://doi.org/10.1038/nmeth1113
11. Subramanian, A., Tamayo, P., Mootha, V. K., Mukherjee, S., Ebert, B. L., Gillette, M. A., Paulovich, A., Pomeroy, S. L., Golub, T. R., Lander, E. S., & Mesirov, J. P. (2005). Gene set enrichment analysis: A knowledge-based approach for interpreting genome-wide expression profiles. *Proceedings of the National Academy of Sciences of the United States of America*, *102*, 15545–15550. https://doi.org/10.1073/pnas.0506580102
12. Mootha, V. K., Lindgren, C. M., Eriksson, K.-F., Subramanian, A., Sihag, S., Lehar, J., Puigserver, P., Carlsson, E., Ridderstråle, M., Laurila, E., Houstis, N., Daly, M. J., Patterson, N., Mesirov, J. P., Golub, T. R., Tamayo, P., Spiegelman, B., Lander, E. S., Hirschhorn, J. N., … Groop, L. C. (2003). PGC-1α-responsive genes involved in oxidative phosphorylation are coordinately downregulated in human diabetes. *Nature Genetics*, *34*, 267–273. https://doi.org/10.1038/ng1180
13. Liberzon, A., Birger, C., Thorvaldsdóttir, H., Ghandi, M., Mesirov, J. P., & Tamayo, P. (2015). The molecular signatures database hallmark gene set collection. *Cell Systems*, *1*, 417–425. https://doi.org/10.1016/j.cels.2015.12.004
14. Liberzon, A., Subramanian, A., Pinchback, R., Thorvaldsdóttir, H., Tamayo, P., & Mesirov, J. P. (2011). Molecular signatures database (MSigDB) 3.0. *Bioinformatics (Oxford, England)*, *27*, 1739–1740. https://doi.org/10.1093/bioinformatics/btr260
15. RCoreTeam. (2023). *R: A language and environment for statistical computing journal*. R Foundation for Statistical Computing. https://www.R-project.org
16. Wu, T., Hu, E., Xu, S., Chen, M., Guo, P., Dai, Z., Feng, T., Zhou, L., Tang, W., Zhan, L., Fu, X., Liu, S., Bo, X., & Yu, G. (2021). clusterProfiler 4.0: A universal enrichment tool for interpreting omics data. *Innovation (Cambridge (Mass.))*, *2*, 100141. https://doi.org/10.1016/j.xinn.2021.100141
17. Yu, G. (2023). enrichplot: Visualization of Functional Enrichment Result. Journal, doi: 10.18129/B9.bioc.enrichplot
18. Kohno, T., Sorgente, N., Ishibashi, T., Goodnight, R., & Ryan, S. J. (1987). Immunofluorescent studies of fibronectin and laminin in the human eye. *Investigative Ophthalmology & Visual Science*, *28*, 506–514. https://www.ncbi.nlm.nih.gov/pubmed/3549611
19. Pang, X., He, X., Qiu, Z., Zhang, H., Xie, R., Liu, Z., Gu, Y., Zhao, N., Xiang, Q., & Cui, Y. (2023). Targeting integrin pathways: mechanisms and advances in therapy. *Signal Transduction and Targeted Therapy*, *8*, 1. https://doi.org/10.1038/s41392-022-01259-6
20. Ogden, A. T., Nunes, I., Ko, K., Wu, S., Hines, C. S., Wang, A.-F., Hegde, R. S., & Lang, R. A. (1998). GRIFIN, a novel lens-specific protein related to the galectin family. *The Journal of Biological Chemistry*, *273*, 28889–28896. https://doi.org/10.1074/jbc.273.44.28889
21. García Caballero, G., Kaltner, H., Michalak, M., Shilova, N., Yegres, M., André, S., Ludwig, A.-K., Manning, J. C., Schmidt, S., Schnölzer, M., Bovin, N. V., Reusch, D., Kopitz, J., & Gabius, H.-J. (2016). Chicken GRIFIN: A homodimeric member of the galectin network with canonical properties and a unique expression profile. *Biochimie*, *128–129*, 34–47. https://doi.org/10.1016/j.biochi.2016.06.001
22. Ahmed, H., & Vasta, G. R. (2008). Unlike mammalian GRIFIN, the zebrafish homologue (DrGRIFIN) represents a functional carbohydrate-binding galectin. *Biochemical and Biophysical Research Communications*, *371*, 350–355. https://doi.org/10.1016/j.bbrc.2008.04.078
23. Robinson, R., Youngblood, H., Iyer, H., Bloom, J., Lee, T. J., Chang, L., Lukowski, Z., Zhi, W., Sharma, A., & Sharma, S. (2020). Diabetes induced

alterations in murine vitreous proteome are mitigated by IL-6 trans-signaling inhibition. *Investigative Ophthalmology & Visual Science*, *61*, 2. https://doi.org/10.1167/iovs.61.11.2

24. Hetz, C. (2012). The unfolded protein response: controlling cell fate decisions under ER stress and beyond. *Nature Reviews Molecular Cell Biology*, *13*, 89–102. https://doi.org/10.1038/nrm3270
25. Nsiah-Sefaa, A., & Mckenzie, M. (2016). Combined defects in oxidative phosphorylation and fatty acid β-oxidation in mitochondrial disease. *Bioscience Reports*, *36*, https://doi.org/10.1042/BSR20150295
26. Gong, Q., Wang, H., Yu, P., Qian, T., & Xu, X. (2021). Protective or harmful: The dual roles of autophagy in diabetic retinopathy. *Autophagy in Diabetic Retinopathy Journal*, *8*, 644121. https://doi.org/10.3389/fmed.2021.644121
27. Hu, L., Lv, X., Li, D., Zhang, W., Ran, G., Li, Q., & Hu, J. (2021). The anti-angiogenesis role of FBXW7 in diabetic retinopathy by facilitating the ubiquitination degradation of c-Myc to orchestrate the HDAC2. *Journal of Cellular and Molecular Medicine*, *25*, 2190–2202. https://doi.org/10.1111/jcmm.16204
28. Shi, Y., Xu, X., Zhang, Q., Fu, G., Mo, Z., Wang, G. S., Kishi, S., & Yang, X.-L. (2014). tRNA synthetase counteracts c-Myc to develop functional vasculature. *eLife*, *3*, e02349. https://doi.org/10.7554/eLife.02349
29. Bae, S., Oh, B., Tsai, J., Park, P. S. U. K., Greenblatt, M. B., Giannopoulou, E. G., & Park-Min, K.-H. (2022). The crosstalk between MYC and mTORC1 during osteoclastogenesis. *Frontiers in Cell and Developmental Biology*, *10*, 920683. https://doi.org/10.3389/fcell.2022.920683
30. Yoshioka, M., Kayo, T., Ikeda, T., & Koizuni, A. (1997). A novel locus, Mody4, distal to D7Mit189 on chromosome 7 determines early-onset NIDDM in nonobese C57BL/6 (Akita) mutant mice. *Diabetes*, *46*, 887–894. https://doi.org/10.2337/diab.46.5.887
31. Herbach, N., Rathkolb, B., Kemter, E., Pichl, L., Klaften, M., De Angelis, M. H., Halban, P. A., Wolf, E., Aigner, B., & Wanke, R. (2007). Dominant-negative effects of a novel mutated Ins2 allele causes early-onset diabetes and severe β-cell loss in Munich Ins2 C95S mutant mice. *Diabetes*, *56*, 1268–1276. https://doi.org/10.2337/db06-0658
32. Renner, S., Dobenecker, B., Blutke, A., Zöls, S., Wanke, R., Ritzmann, M., & Wolf, E. (2016). Comparative aspects of rodent and nonrodent animal models for mechanistic and translational diabetes research. *Theriogenology*, *86*, 406–421. https://doi.org/10.1016/j.theriogenology.2016.04.055
33. Loukovaara, S., Nurkkala, H., Tamene, F., Gucciardo, E., Liu, X., Repo, P., Lehti, K., & Varjosalo, M. (2015). Quantitative proteomics analysis of vitreous humor from diabetic retinopathy patients *Diabetic Retinopathy Patients Journal*, *14*, 5131–5143. https://doi.org/10.1021/acs.jproteome.5b00900
34. Park, S. W., Yun, J.-H., Kim, J. H., Kim, K.-W., Cho, C.-H., & Kim, J. H. (2014). Angiopoietin 2 induces pericyte apoptosis via α3β1 integrin signaling in diabetic retinopathy. *Diabetes*, *63*, 3057–3068. https://doi.org/10.2337/db13-1942
35. Silva, R., D'amico, G., Hodivala-Dilke, K. M., & Reynolds, L. E. (2008). Integrins: The keys to unlocking angiogenesis. *Arteriosclerosis, Thrombosis, and Vascular Biology*, *28*, 1703–1713. https://doi.org/10.1161/ATVBAHA.108.172015
36. Hu, T.-T., Vanhove, M., Porcu, M., Van Hove, I., Van Bergen, T., Jonckx, B., Barbeaux, P., Vermassen, E., & Feyen, J. H. M. (2019). The potent small molecule integrin antagonist THR-687 is a promising next-generation therapy for retinal vascular disorders. *Experimental Eye Research*, *180*, 43–52. https://doi.org/10.1016/j.exer.2018.11.022
37. Wilkinson-Berka, J. L., Alousis, N. S., Kelly, D. J., & Gilbert, R. E. (2003). COX-2 inhibition and retinal angiogenesis in a mouse model of retinopathy of prematurity. *Investigative Ophthalmology & Visual Science*, *44*, 974–979. https://doi.org/10.1167/iovs.02-0392
38. Madonna, R., Giovannelli, G., Confalone, P., Renna, F. V., Geng, Y.-J., & De Caterina, R. (2016). High glucose-induced hyperosmolarity contributes to COX-2 expression and angiogenesis: Implications for diabetic retinopathy. *Cardiovascular Diabetology*, *15*, 18. https://doi.org/10.1186/s12933-016-0342-4
39. Song, X.-L., Li, M.-J., Liu, Q., Hu, Z.-X., Xu, Z.-Y., Li, J.-H., Zheng, W.-L., Huang, X.-M., Xiao, F., Cui, Y.-H., & Pan, H.-W. (2020). Cyanidin-3-O-glucoside protects lens epithelial cells against high glucose-induced apoptosis and prevents cataract formation via suppressing NF-κB activation and Cox-2 expression. *Journal of Agricultural and Food Chemistry*, *68*, 8286–8294. https://doi.org/10.1021/acs.jafc.0c03194
40. García Caballero, G., Schmidt, S., Schnölzer, M., Schlötzer-Schrehardt, U., Knospe, C., Ludwig, A.-K., Manning, J. C., Muschler, P., Kaltner, H., Kopitz, J., & Gabius, H.-J. (2019). Chicken GRIFIN: Binding partners, developmental course of localization and activation of its lens-specific gene expression by L-Maf/Pax6. *Cell and Tissue Research*, *375*, 665–683. https://doi.org/10.1007/s00441-018-2931-x
41. Barton, K. A., Hsu, C.-D., & Petrash, J. M. (2009). Interactions between small heat shock protein α-crystallin and galectin-related interfiber protein (GRIFIN) in the ocular lens. *Biochemistry*, *48*, 3956–3966. https://doi.org/10.1021/bi802203a
42. Hetz, C., Zhang, K., & Kaufman, R. J. (2020). Mechanisms, regulation and functions of the unfolded protein response. *Nature Reviews. Molecular Cell Biology*, *21*, 421–438. https://doi.org/10.1038/s41580-020-0250-z
43. Mulhern, M. L., Madson, C. J., Danford, A., Ikesugi, K., Kador, P. F., & Shinohara, T. (2006). The unfolded protein response in lens epithelial cells from galactosemic rat lenses. *Investigative Ophthalmology & Visual Science*, *47*, 3951–3959. https://doi.org/10.1167/iovs.06-0193
44. Mazzoli, V., Zhong, L. H., Dang, V. T., Shi, Y., & Werstuck, G. H. (2020). Characterization of retinal microvascular complications and the effects of endoplasmic reticulum stress in mouse models of diabetic atherosclerosis. *Diabetic Atherosclerosis Journal*, *61*, 49. https://doi.org/10.1167/iovs.61.10.49
45. Zhong, Y., Li, J., Chen, Y., Wang, J. J., Ratan, R., & Zhang, S. X. (2012). Activation of endoplasmic reticulum stress by hyperglycemia is essential for Müller cell–derived inflammatory cytokine production in diabetes. *Diabetes*, *61*, 492–504. https://doi.org/10.2337/db11-0315
46. Rosarda, J. D., Giles, S., Harkins-Perry, S., Mills, E. A., Friedlander, M., Wiseman, R. L., & Eade, K. T. (2023). Imbalanced unfolded protein response signaling contributes to 1-deoxysphingolipid retinal toxicity. *Nature Communications*, *14*, 4119. https://doi.org/10.1038/s41467-023-39775-w
47. Chen, Y., Coorey, N. J., Zhang, M., Zeng, S., Madigan, M. C., Zhang, X., Gillies, M. C., Zhu, L., & Zhang, T. (2022). Metabolism dysregulation in retinal diseases and related therapies. *Antioxidants (Basel, Switzerland)*, *11*, 942. https://doi.org/10.3390/antiox11050942
48. Van Hove, I., De Groef, L., Boeckx, B., Modave, E., Hu, T.-T., Beets, K., Etienne, I., Van Bergen, T., Lambrechts, D., Moons, L., Feyen, J. H. M., & Porcu, M. (2020). Single-cell transcriptome analysis of the Akimba mouse retina reveals cell-type-specific insights into the pathobiology of diabetic retinopathy. *Diabetologia*, *63*, 2235–2248. https://doi.org/10.1007/s00125-020-05218-0
49. Oh, J. K., Lima De Carvalho, J. R., Nuzbrokh, Y., Ryu, J., Chemudupati, T., Mahajan, V. B., Sparrow, J. R., & Tsang, S. H. (2020). Retinal manifestations of mitochondrial oxidative phosphorylation disorders. *Investigative Ophthalmology & Visual Science*, *61*, 12. https://doi.org/10.1167/iovs.61.12.12
50. Umetsu, A., Furuhashi, M., Watanabe, M., Ohkawa, E., Tsugeno, Y., Suzuki, S., Itoh, K., Ida, Y., Hikage, F., & Ohguro, H. (2022). Fatty acid metabolism is involved in both retinal physiology and the pathology of retinal vascular diseases. *Prostaglandins, Leukotrienes, and Essential Fatty Acids*, *183*, 102473. https://doi.org/10.1016/j.plefa.2022.102473
51. Gwinn, D. M., Shackelford, D. B., Egan, D. F., Mihaylova, M. M., Mery, A., Vasquez, D. S., Turk, B. E., & Shaw, R. J. (2008). AMPK phosphorylation of raptor mediates a metabolic checkpoint. *Molecular Cell*, *30*, 214–226. https://doi.org/10.1016/j.molcel.2008.03.003

52. Hara, T., Nakamura, K., Matsui, M., Yamamoto, A., Nakahara, Y., Suzuki-Migishima, R., Yokoyama, M., Mishima, K., Saito, I., Okano, H., & Mizushima, N. (2006). Suppression of basal autophagy in neural cells causes neurodegenerative disease in mice. *Nature*, *441*, 885–889. https://doi.org/10.1038/nature04724
53. Zhang, J., Chen, C., Wu, L., Wang, Q., Chen, J., Zhang, S., & Chen, Z. (2019). C-myc contributes to the release of Müller cells-derived proinflammatory cytokines by regulating lncRNA MIAT/XNIP pathway. *The International Journal of Biochemistry & Cell Biology*, *114*, 105574. https://doi.org/10.1016/j.biocel.2019.105574
54. Perez-Riverol, Y., Bai, J., Bandla, C., García-Seisdedos, D., Hewapathirana, S., Kamatchinathan, S., Kundu, D. J., Prakash, A., Frericks-Zipper, A., Eisenacher, M., Walzer, M., Wang, S., Brazma, A., & Vizcaíno, J. A. (2022). The PRIDE database resources in 2022: A hub for mass spectrometry-based proteomics evidences. *Nucleic Acids Research*, *50*, D543–D552. https://doi.org/10.1093/nar/gkab1038

SUPPORTING INFORMATION

Additional supporting information may be found online https://doi.org/10.1002/pmic.202300591 in the Supporting Information section at the end of the article.

How to cite this article: Degroote, R. L., Schmalen, A., Renner, S., Wolf, E., Hauck, S. M., & Deeg, C. A. (2024). Diabetic retinopathy from the vitreous proteome perspective: The *INS*^{C94Y} transgenic pig model study. *Proteomics*, e2300591. https://doi.org/10.1002/pmic.202300591